The Plastic Deformation of TiAl

D. SHECHTMAN, M. J. BLACKBURN, AND H. A. LIPSITT

The deformation substructure of TiAl (Llo type ordered lattice) tested in compression, and the factors determining it were investigated. Two types of dislocations take part in the plastic deformation, namely a/2[110] and a/2[011]. The latter type will disorder the Llo superlattice and therefore would be expected to move in pairs as superdislocations. Some observations are essentially in agreement with the predictions, however the large proportion and morphology of a/2[011] dislocations observed was unexpected. Twins of the [112](11$\bar{1}$) type play an important role in the deformation of the alloy, and the early stages of their formation have been recorded. Finally, equi-Schmid factor lines have been constructed in an attempt to evaluate the importance of the sense of the applied stress on the deformation capability of the alloy.

THREE intermetallic compounds or ordered structures occur in the titanium aluminum system based on the compositions Ti_3Al (α_2-phase), TiAl (γ phase) and $TiAl_3$. Both the α_2 phase and the γ-phase have potential as materials for use at elevated temperatures and some development work has been performed.[1] Within this laboratory, it was decided to reinvestigate the potential of alloys based on TiAl and at almost the same time, the Pratt and Whitney Company (Florida) embarked on a similar program. Both programs are continuing in parallel and this paper reports some initial results obtained on the plastic deformation behavior of the γ-phase at ambient temperatures.

The starting point for these studies is the results obtained by the Armour Research Foundation Institute (now Illinois Institute of Technology) which are summarized in a paper by McAndrew and Kessler.[1] It was shown that the compound TiAl and some dilute alloys with a TiAl base exhibited creep and oxidation properties at 950°C which were far in excess of the values for conventional titanium alloys. These observations coupled with the high modulus and low density of the γ-phase, raise the question of why the material is not presently used. The answer is two-fold; first, the room temperature tensile ductility is essentially zero, and second, the formability characteristics even at high temperatures are not particularly good except when performed at slow strain rate. The lack of ductility is surprising at first sight, for the γ-phase has an Llo structure with an axial ratio of 1.02, and thus is essentially face centered cubic; it also has rather low hardness at room temperature, approximately 200 DPH. Comparable Llo structures formed in CuAu and CoPt do exhibit tensile ductility at room temperature after treatments designed to produce a high degree of order. In these phases, however, an order-disorder reaction occurs in the solid state, whereas TiAl is ordered to its (incongruent) melting point. The γ-phase can be deformed in compression at room temperature and strains of about 8 pct with no cracking have been obtained.

This paper will consider in some detail the glide process that occurs in the γ-phase deformed in compression at room temperature. The nature of the dislocations in the Llo structure was speculated upon by Marcinkowski *et al.*[2] Two possible a/2⟨110⟩ slip vectors may exist on the {111} plane. The first is a/2[110] which is divided into two partials, a/6[211] + a/6[12$\bar{1}$]. Between the two partials there is a region of stacking fault and antiphase domain boundary, but after the second partial, the structure is restored again, (Fig. 1). The second type of dislocation is a/2[011]. It is divided into two partials a/6[121] + a/6[$\bar{1}$12]. When the leading partial is the a/6[$\bar{1}$12], there is a stacking fault region between the two partials, however, when the a/6[121] partial passes, the superlattice is not reformed; a region of antiphase domain boundary is formed. Coupled slip of a second a/2[011] dislocation will leave the superlattice undisturbed (Fig. 2). The a/2[011] dislocations are predicted, therefore, to slip in pairs, which intuitively may be considered a more difficult process. We shall refer to a/2[110] dislocations as "easy" slip type and to a/2[011] dislocations as "hard" slip type.

Some observations of the dislocations that take part in the plastic deformation of TiAl were made by Cass and Spencer.[3] They reported a/2[110] dislocations and (111) mechanical twins, similar twins were also reported to be a predominant deformation mode for CuAu by Pashley *et al.*[4]

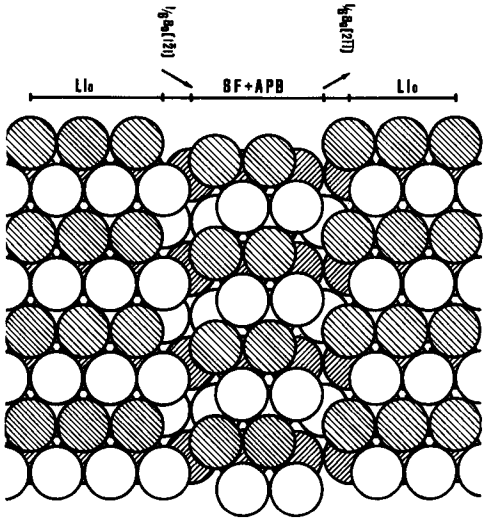

Fig. 1—Atomic arrangement on two successive (111) planes of the Llo lattice showing an a/2[1$\bar{1}$0](111) dislocation.

D. SHECHTMAN and H. A. LIPSITT are N.R.C. Postdoctoral Associate and Group Leader respectively at the Metallurgy and Ceramics group of the Aerospace Research Labs, Wright-Patterson Air Force Base, Ohio 45433. M. J. BLACKBURN, formerly visiting Scientist at the Aerospace Research Laboratories, is now a Group Leader at Pratt & Whitney Aircraft, East Hartford, Connecticut.

Manuscript submitted August 24, 1973.

EXPERIMENTAL PROCEDURE

Two alloys of the γ structure were prepared, the nominal compositions of which were: Ti-36 wt pct Al (50 at. pct) and Ti-40 wt pct Al, (54 at. pct) (compositions in Table I). The first alloy was fabricated by P and W in cooperation with the Air Force Materials Laboratory which also extruded the second alloy. The fabrication process of the alloys started by casting an ingot of the desired composition. The ingot was homogenized for seven days at 1000°C and then powdered, canned in a titanium can and extruded. The extrusions were annealed at 1000°C for seven days in vacuum, and then stressed at room temperature in compression in an Instron tensile machine at the rate of 0.05 a inch/min to strains $\leqq 8$ pct. Specimens for electron microscopy were cut at 45 deg to the compression axis and the foils were prepared by standard methods,[5] electropolishing was performed at -50°C and at constant current density of 0.3 amp/cm^2. (The thin foils were examined in a Philips E. M. 300, operated at 100 kV.)

RESULTS

1. Phase Structures

It was initially intended to study the deformation modes in the Ti:36 pct Al alloy as most of the available mechanical property data had been generated for this material. However, this alloy was found to contain two phases after all annealing treatments ($T \leq 1350$°C); the two phases α_2 (Ti_3Al) and γ (TiAl) are shown in Fig. 3. This structure, phase morphology and orientation relationship are very similar to that observed in a Ti-26 pct Al alloy at the other end of the two phase region.[6] No evidence for a $(\alpha_2+\beta)$ phase field has been found indicating that the Ence and Marolin[7] phase diagram in this region has the correct shape, however, the position of the $\alpha_2+\gamma$ (labelled $\epsilon+\gamma$) phase line is incorrect. Thus, for ease of analysis, it was decided to concentrate on the Ti-40 pct Al alloy which was found to be single phase after all treatments, (a typical microstructure is shown in Fig. 4). Further, there was no evidence of the {110} growth twins typical of solid state Llo order-disorder transformations, although {111} annealing twins were quite common. Thus, the basic microstructure was rather like a low stacking fault energy face centered cubic material and therefore an ideal structure for studying deformation substructure.

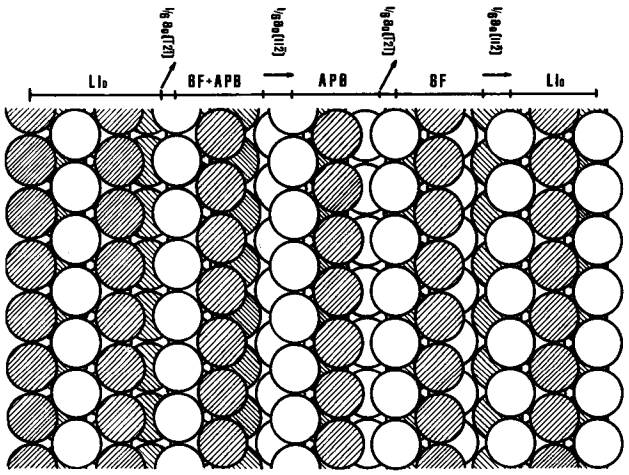

Fig. 2—Atomic arrangement on two successive (111) planes of the Llo lattice showing two a/2 [01$\bar{1}$](111) dislocations.

2. Deformed Structures

a) Before discussing the features of the deformation, a basic framework for the analysis of dislocations and so forth, in the γ-phase was established. A series of preliminary calculations were performed which are summarized below. The lattice parameters of the γ-phase are a = 3.98, c = 4.08 (c/a = 1.02). However, we shall treat the lattice (and its defects) as though it is fcc, *i.e.*, as if c/a = 1. Allowed reflections (*hkl*) from this structure are both fundamental and superlattice reflections and the general rule for observed reflections is *h* and *k* unmixed (as for base centered cubic lattice).

Note that as the structure is slightly tetragonal, the reflections such as (200) and (002) will have slightly

Table I. Composition of the Alloys

Alloy	Al	O, ppm	H, ppm	N, ppm	Fe
I	36.0	587	18	26	0.034
II	40.0	1208	37	39	0.05

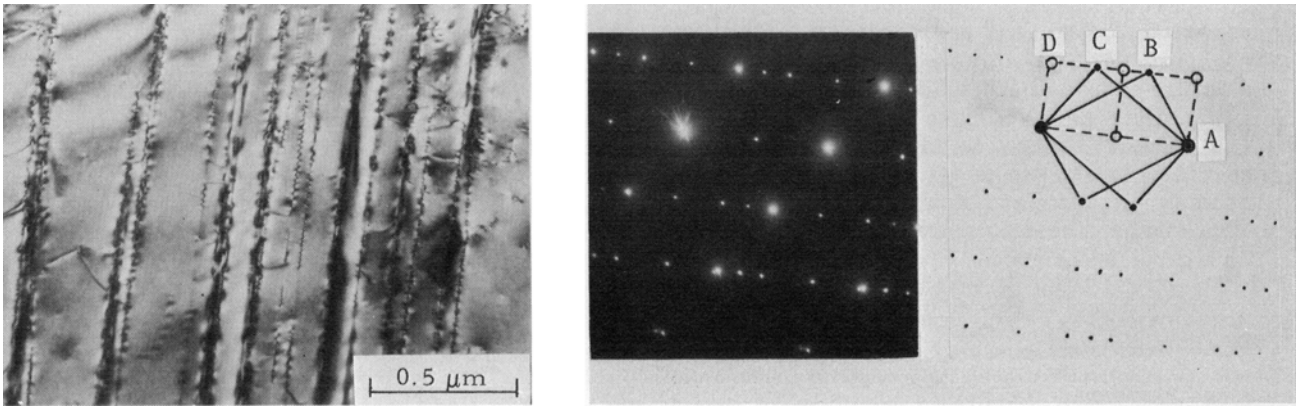

Fig. 3—The Ti-36 wt pct Al consists of γ phase and precipitates of α_2 on $\{111\}_\gamma$ planes. The regions of precipitation are twinned as demonstrated by the diffraction pattern. The pattern is rotation corrected and the diffraction points are: A—(0002)α_2, (111)γ matrix, (111)γ twin. B—(110)γ twin. C—(001)γ matrix. D—($\bar{1}$010)α_2.

different spacings. Further the restrictions on the allowed reflections result in the ability to make unambiguous determination of some burgers vectors, for example a/2[110] can be distinguished from a/2(001].

Calculation of the conditions of visibility of whole and partial dislocations and stacking faults were performed. One important conclusion from these results is that the fringe contrast from a 1/3[111] type fault and the contrast from a/6[112] partial dislocations will not be visible at the same time (using two beam conditions), since the visibility condition for partials in this material is $\bar{g} \cdot \bar{b} = 1$. Extinction distances for the TiAl lattice were computed for fundamental and superlattice reflections and the results are presented in Table II.

The antiphase domain boundary (APB) energy for the {111} plane of the phase lattice was calculated using the quasichemical approach detailed by Marcin-

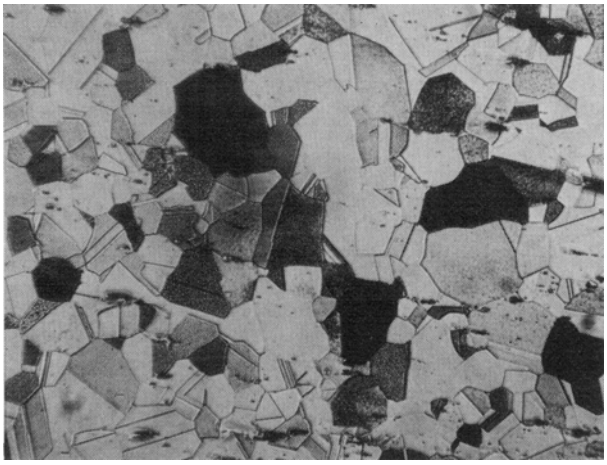

Fig. 4—Ti-40 wt pct Al. Magnification 75 times.

Table II. Extinction Distances for TiAl

hkl		to[Å]
001	S	1377
110	S	1854
111	F	446
002	F	512
200	F	524
201	S	2410
112	S	2410
202	F	790
220	F	790
003	S	3013
221	S	3013
310	S	3214
113	F	964
131	F	964
222	F	1026
023	S	3708
132	S	3444
004	F	1296

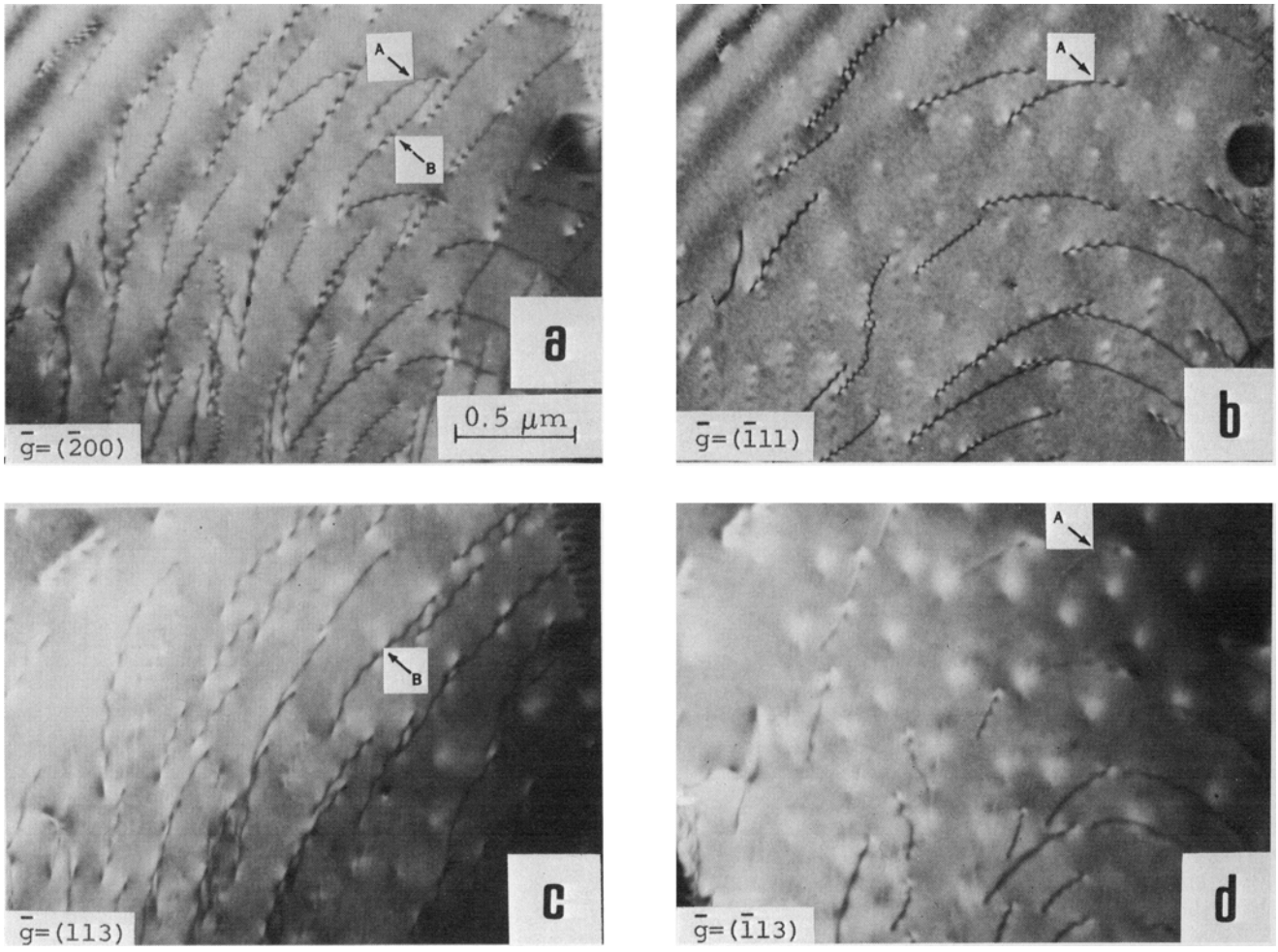

Fig. 5—Array of dislocations in slightly deformed Ti-40 wt pct Al. Set A is a/2[$\bar{1}$10] and B is a/2[110].

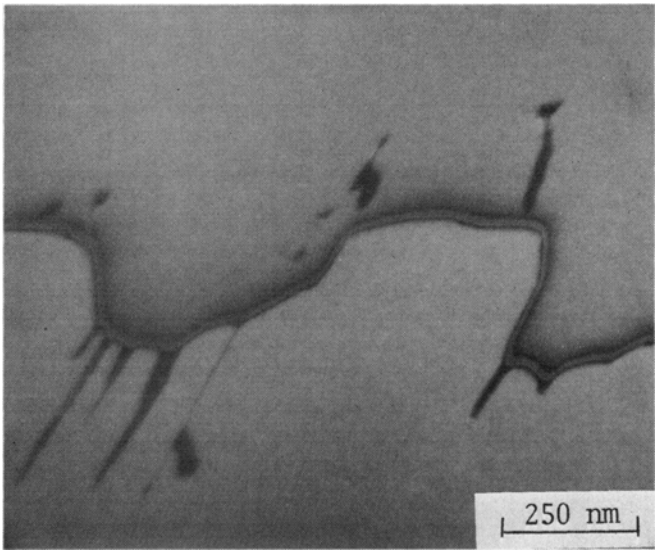

Fig. 6—Pair of a/2[011] dislocations. (Bright field, operating reflection $\bar{g}$ = (111).

kowski.[8] Thus, using the equation for the interaction energy:

$$V_{\text{Llo}} = \frac{kT_c}{0.73}$$

and substituting the value of APB energy per unit area:

$$E_{\text{Llo}}^{\{111\}} = \frac{4V}{a^2\sqrt{3}}$$

$$E_{\text{Llo}}^{\{111\}} = \frac{4kT_c}{0.73\,a^2\sqrt{3}}$$

(where T_c = the critical ordering temperature was taken as the melting temperature = 1723 K) a value of 470 ergs/cm^2 is obtained.

In the following descriptions of the deformation substructure, we shall emphasize the general features rather than give a fully detailed analysis of the contrast experiments performed. In all cases at least two zones and six reflections were utilized in the determination of dislocation, fault and twin vectors, but in order to keep the number of micrographs within reasonable bounds only selected illustrations will be used.

b) Observations of Specific Dislocation Types. Numerous dislocations of a/2[110] type have been observed after deformation, examples are shown in Fig. 5(*a*), (*b*), (*c*) which also illustrate the vector determination. No evidence for the dissociation of an a/2[110] into its constituent a/6[211] a/6[12$\bar{1}$] partials connected by a ribbon of stacking fault and APB has been obtained. The distribution of such dislocations tends to be relatively random and only a few examples of planar groupings have been observed. This type of dislocation is also a common constituent of sub-boundaries occasionally found in this material.

The second type of complete dislocation that could be expected to occur are of the a/2[011] or a/2[101] type. Marcinkowski[8] has predicted that such dislocations should move as superdislocation pairs as a single dislocation produces an APB in the Llo lattice. The actual superdislocation could be more complicated if dissociation into partials were to occur, but we shall defer discussion of this process to the next section. In practice, a large number of dislocations of the a/2[011] type are observed in deformed TiAl samples, although the structure and contrast behavior of these dislocations only partially fulfill the predictions of Marcinkowski. The morphological and contrast characteris-

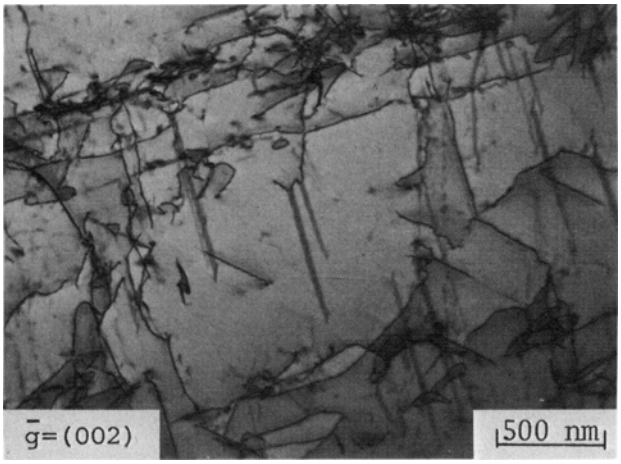

(*a*)

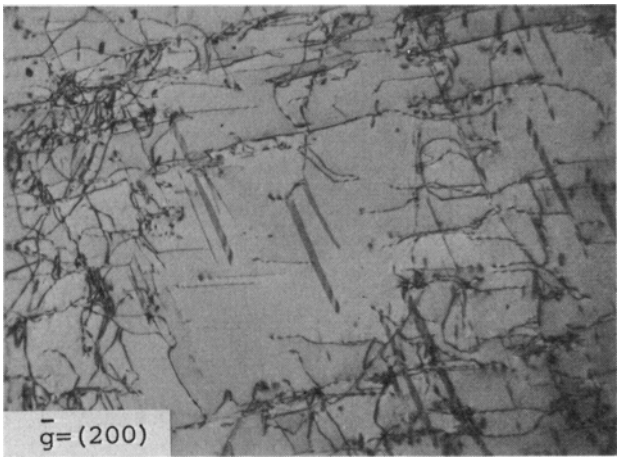

(*b*)

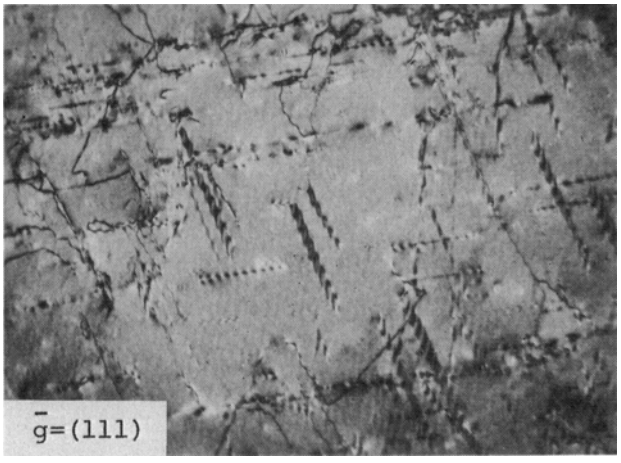

(*c*)

Fig. 7—a/2[$\bar{1}$01] dislocations play an important role in the plastic deformation of the Ti–40 wt pct Al. Only a small proportion of the dislocations (invisible for $\bar{g}$ = 002) are of the a/2[110] type.

tics of these dislocations can be summarized as follows.

The dislocations sometimes appeared as single lines, but, complex configurations such as pairs occur more commonly (Fig. 6).

Contrast analysis indicated that the dislocations have a [101] vector rather than a/6[414] (Fig. 7) (See discussion).

In some cases, the dislocations are associated with stacking faults (discussed in some detail below).

Numerous attempts to resolve APB's associated with such dislocations were unsuccessful. No defect which could be unambiguously identified as an APB has been observed at this time, even though the extinction distances for the reflections used (Table II) should have enabled such observation

c) Observation of Stacking Faults and Twins. Other

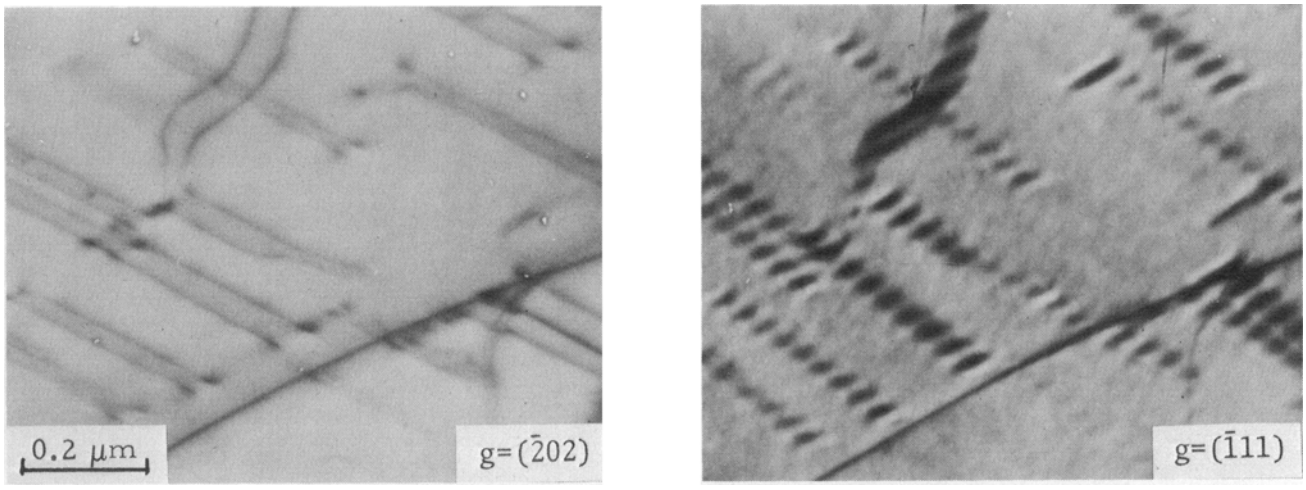

Fig. 8—a/3 [111] stacking faults (bright field, operating reflections marked).

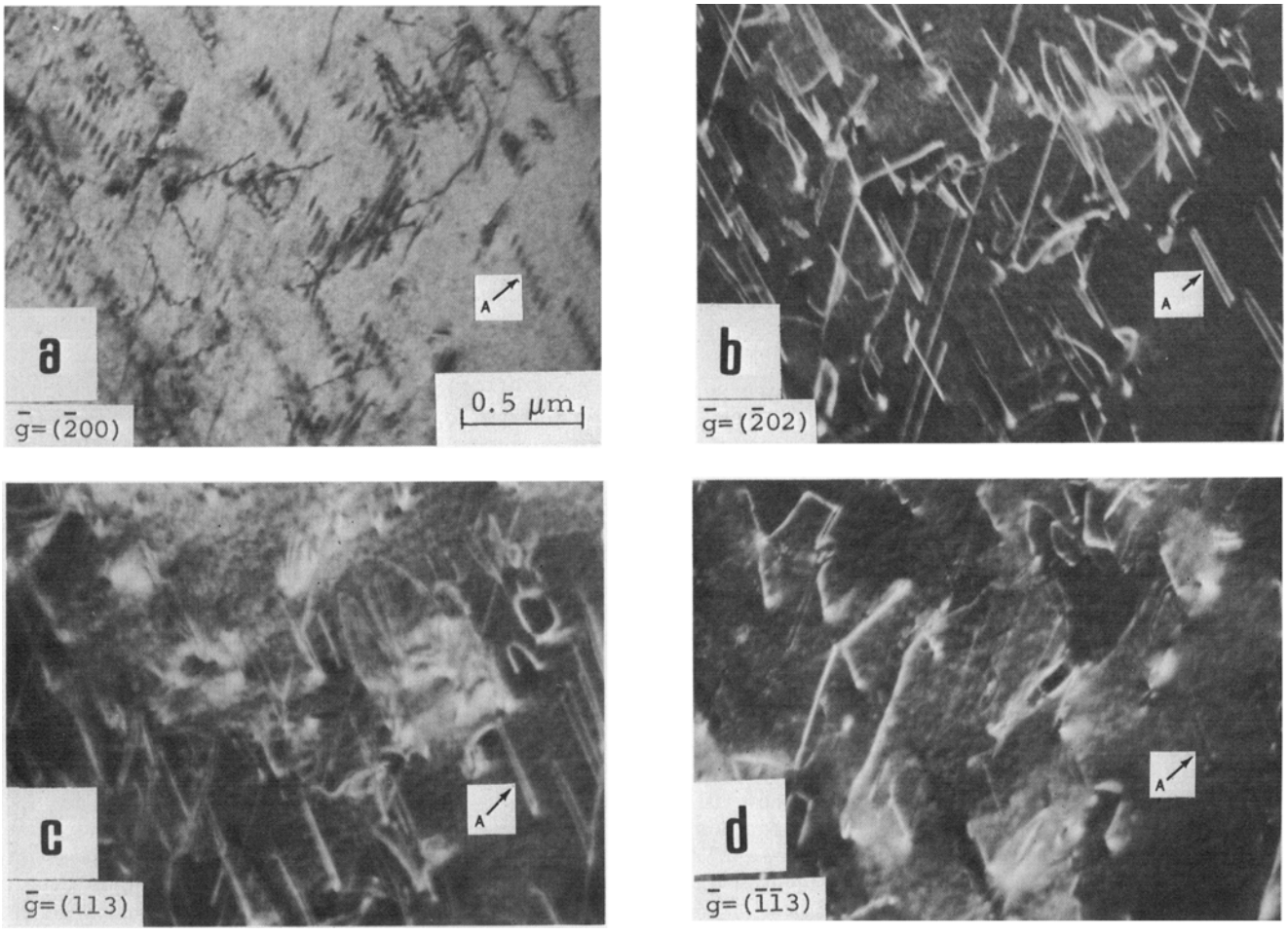

Fig. 9—a/3 [111] stacking faults bounded by a/6 [112] partial dislocations. At (*a*), the stacking fault contrast is seen but not the contrast from the dislocations. At (*b*), (*c*), and (*d*) only contrast from the partials is resolved. (Stacking fault contrast disappears only for $\bar{g} \cdot \bar{R}$ = integer; contrast from the partials appears only for $\bar{g} \cdot \bar{b}$ = non zero integer).

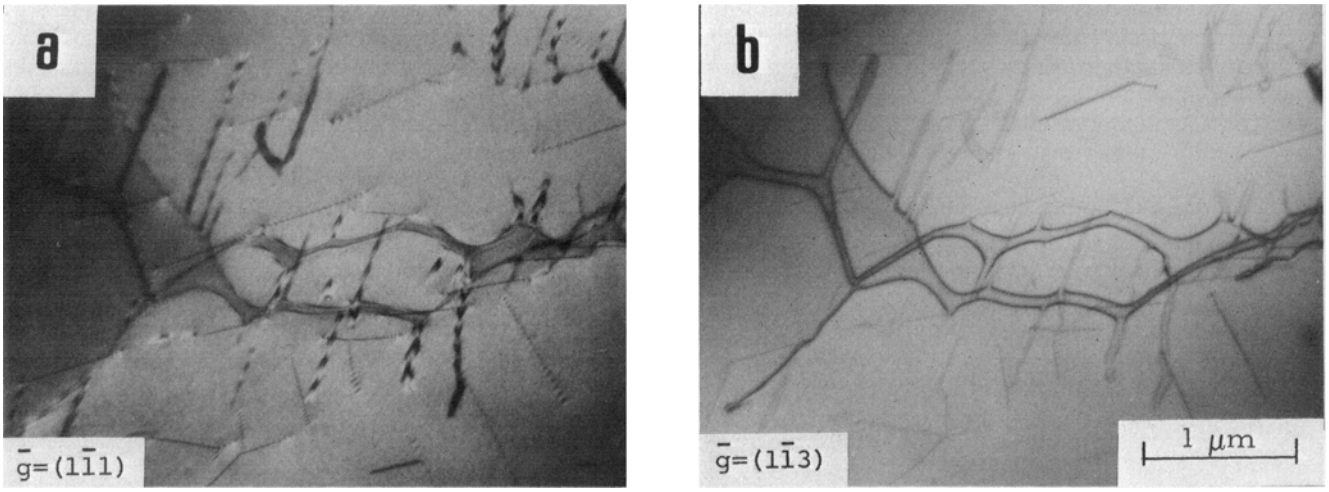

Fig. 10—a/6 [11$\bar{2}$] partial dislocations loops are derived from a/2 [10$\bar{1}$] dislocations. Contrast from the stacking fault is resolved at (*a*), while that from the partial is resolved at (*b*).

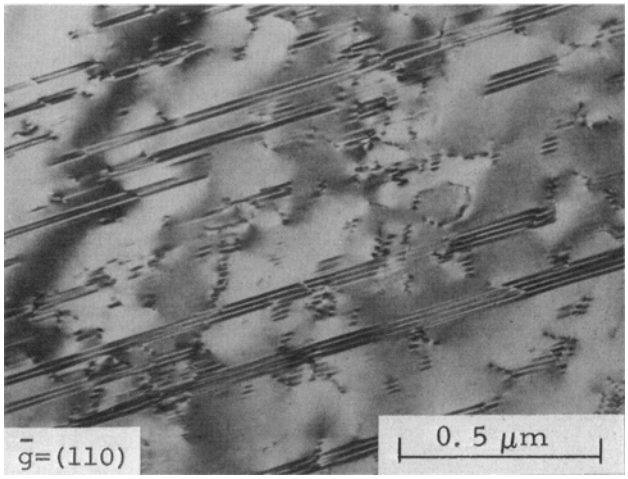

Fig. 11—a/3 [111] stacking faults extend at an early stage of deformation. These extended faults will be developed into [111] twins.

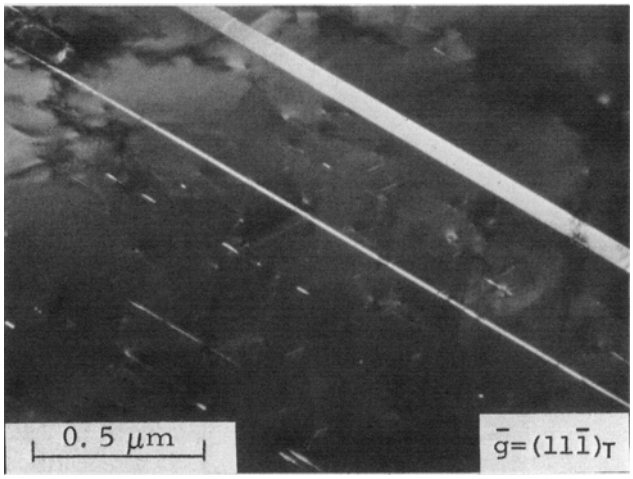

Fig. 12—Twin thicknesses ranging from faults to relatively thicker [111] deformation twins.

prominent features of the deformation structure were the numerous faults observed, *e.g.*, Fig. 8. These faults were shown to be formed on {111} planes by trace analysis and were identified as a/3 [111] type using contrast experiments. The bounding dislocations were shown to be of the type a/6 [112] and only this type, *i.e.*, the fault fraction observed in the microscope, was not bounded by a/6 [211] and so forth, thus, the dislocations that bounded the faults were of the same vector as shown in Fig. 9. The mode of formation of these loops was isolated in several foils and is illustrated in Figs. 10(*a*) and 10(*b*) in which it can be seen that one partial derived from an a/2 [101] dislocation expands into these faulted loops. Further growth of these faults occur as deformation proceeds, as may be seen from Fig. 11 in which several loops now fill the field. It should be emphasized that these faults are not formed by the characteristic separation of a/2 [101] into constituent a/6 [211] and a/6 [1$\bar{1}$2] dislocations, as observed in many face centered cubic alloys with low stacking fault energy, but are formed by the movement of only the a/6 [112] segment. It is not clear if the faults are formed by the expansion of loops under the applied shear stress or are drawn out by the pinning of the a/6 [112] segments of an a/2 [101] dislocation.

In addition to such stacking faults, twins are also formed at a relatively early stage of the deformation process. Fig. 12 illustrates the many twin thicknesses observed, ranging from faults (which are embryonic twins) to twins which are relatively large. These twins are identified as (111) [1$\bar{1}$2] type and only of this type, *e.g.*, the diffraction pattern, Fig. 13, can only be obtained for this specific twin. Thus, the twins are exactly the same as those observed in CuAu, by Pashley *et al.*[4] who also pointed out that the other potential twin system, *e.g.*, (111) [211] destroys the Llo symmetry of the lattice. Other characteristics of these twins have been established and are as expected, thus the twinning plane is (111) and the theoretical shear of 0.713 results in a maximum shear angle of 39 deg 15 min as shown in Fig. 14. Although, we have been unable to clarify the mode of nucleation of the macroscopic twins, it is obvious that the stacking fault loops are potential twin nuclei if some multiplication mechanism (compatible with the Llo structure) could occur. Although virtually all stages of twin thickening have been observed, no real evidence for the transition from

a micro to a macro twin has been obtained. In fact, many large twins appear to nucleate at grain boundaries, inclusions and other twins in the microstructure. However, the growth of twins has been confirmed to occur by the movement of partials at the twin interface. This process can be stimulated by heating the specimen with the microscope and is illustrated by Fig. 15(*a*) (unheated) and 15(*b*) (heated) in which several extra dislocations have moved at points A and B on the upper and lower surface of the twin.

DISCUSSION

Many of the observations made in this preliminary study of TiAl are consistent with the predictions of Marcinkowski[8] for deformation of Llo structures. As

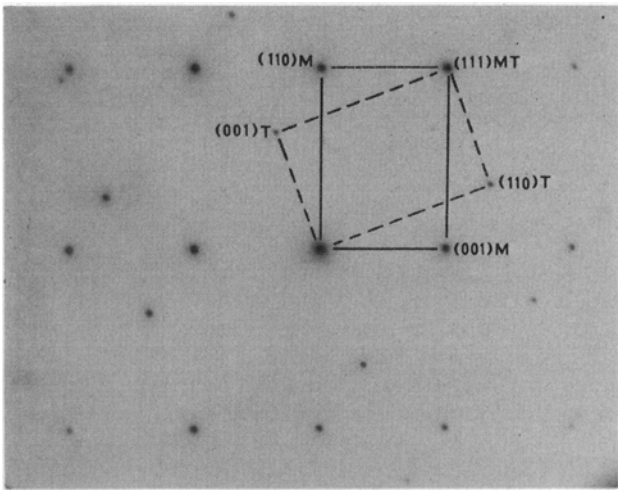

Fig. 13—Diffraction pattern from a twinned structure. This pattern can only be obtained by a [111] ($\bar{1}\bar{1}2$) type twin.

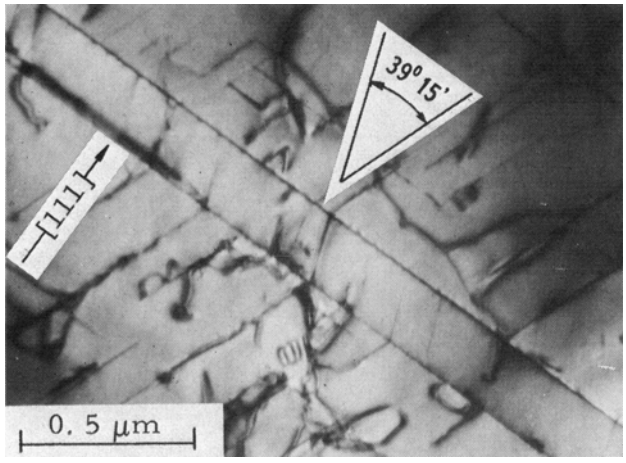

Fig. 14—[111] ($\bar{1}\bar{1}2$) twin observed edge-on ([$\bar{1}$10] zone axis). Shearing angle can be measured from deformed matrix features.

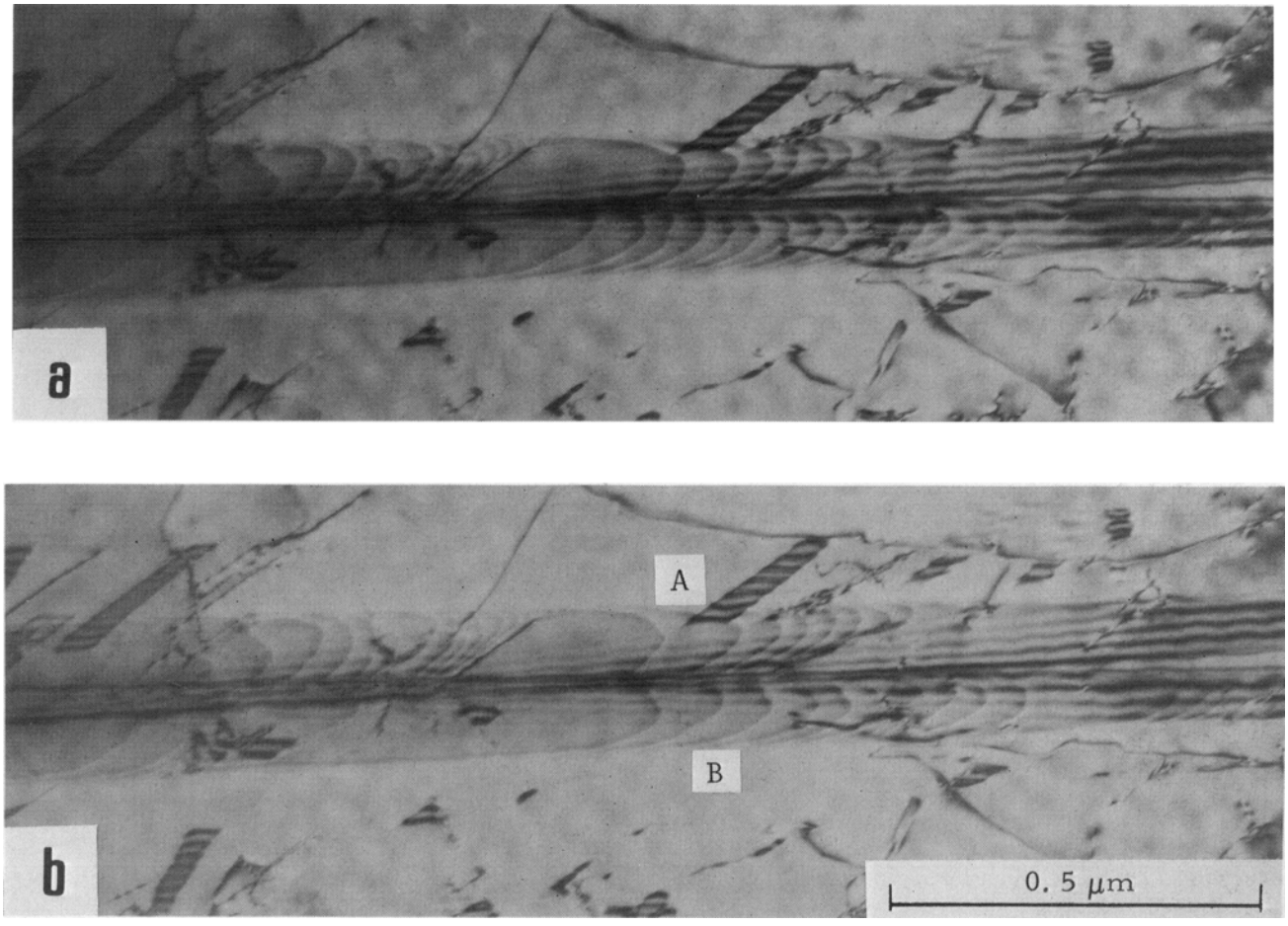

Fig. 15—Movement of partial dislocations on both twin surfaces A and B, stimulated by heating of the foil in the microscope. (*a*) before heating; (*b*) after heating.

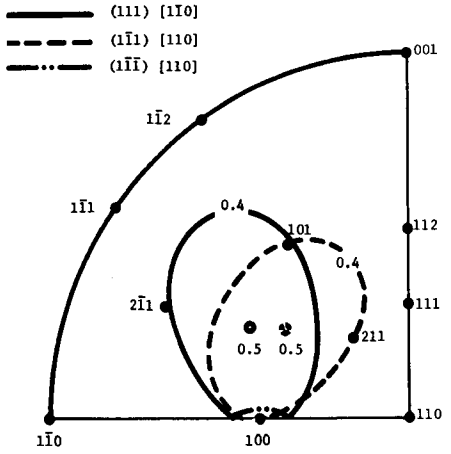

Fig. 16—Equi Schmid factor lines for {111} ⟨110⟩ dislocations, indicating directions along which Schmid factor equals 0.5 and 0.4.

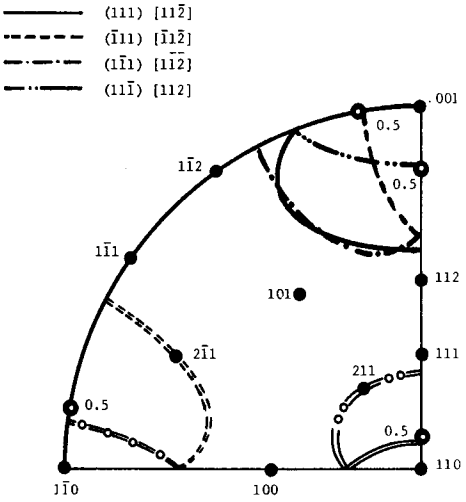

Fig. 17—Equi Schmid factor lines for {111} ⟨112⟩ twinning dislocations. The lines indicate directions along which Schmid factor equals 0.4 and the 0.5 points are also indicated. Single lines are for compression and double lines for tensile load.

the TiAl phase has a high APB energy, one may predict that glide elements which produce no disorder within the lattice would predominate. Thus, the large numbers of a/2[110] dislocation and a/6⟨112⟩ fault defects and the frequency of (111)[11$\bar{2}$] twins are to be expected as these glide processes do not lead to disruption of the ordered structure. The expected separation of the constituent partials of the dissociation

$$a/2[110] \rightarrow a/6[211] + a/6[12\bar{1}]$$

was computed using the equation

$$\frac{Fr}{l} = \frac{\mu}{2\pi r}(\bar{b}_1 \cdot \bar{\xi})(\bar{b}_2 \cdot \bar{\xi}) + \frac{\mu}{2\pi(1-\nu)r}[(\bar{b}_1 \times \bar{\xi}) \cdot (\bar{b}_2 \times \bar{\xi})]$$

where Fr/l is the repulsive force per unit length of the dislocation, ξ is a unit vector in the direction of the dislocation line and r is the separation between the partials. Assuming that the APB energy was considerably greater than the stacking fault energy (which was neglected), the calculated spacings vary from about 9.5Å (screw) to 17.5Å (edge); thus, it is doubtful if the separation could be resolved.

There are several anomalies associated with the "hard" dislocation types which require comment. Al-

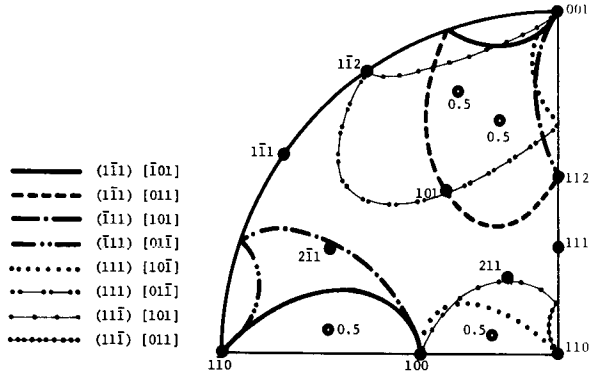

Fig. 18—Equi Schmid factor lines for {111} ⟨011⟩ dislocations. Along the lines, the factor equals 0.4 and points of 0.5 are indicated.

though it has been proven conclusively that such dislocations are a common feature of the deformation substructure, the configuration of such dislocations is rather unclear. The expected structure of an a/2[101] dislocation is illustrated in Fig. 2 in which it is assumed that the leading partial is of the type a/6[112]. The profuse faulting observed, and the numerous annealing twins that occur, both indicate that the stacking fault energy is relatively low (for this vector) in the γ-phase. Thus, one could predict that the leading partial would be separated by some large distance from the other three constituent dislocations of a superdislocation and connected APB ribbons. Further, this closely bound group of three dislocations could behave contrast wise as a composite dislocation of vector a/6[514]. However, the extensive contrast experiments have shown that the dislocations are consistent with a a[101] rather than the composite vector. The low energy a/6[112] dislocation is frequently not observed as widely separated from its generative a/2[101]; instead segments prefer to separate as individual loops. Thus, we are left with the following inconsistencies:

1) Although for various contrast conditions paired dislocations are observed, in many cases for such pairs, the contrast observed is not consistent with both dislocations being of the a/2[011] type. In other words, the pairs do not behave as though they were a simple superdislocation.

2) No APB's have been resolved between such pairs or associated with an apparent single dislocation of the a/2[011] type.

3) The low energy a/6[112] partial (which must be derived from a/2[011] type) does not separate as a unit from the parent dislocation but moves only as small segments in the initial stages of deformation.

The resolution of these apparent problems may well lie in deforming material at different temperatures and in using a computer calculation to predict the expected contrast from a very closely bound dislocation pair, for, as noted above, the contrast from a/2[101] dislocations is certainly different from the a/2[110] type. The computation of the expected separation of an a/2[101] type superdislocation pair is difficult due to the anisotropy of the expected dislocation. The first part of such a calculation is the same as that outlined above for the dissociation of an a/2[110] dislocation which leads to the conclusion that resolution into pairs may be difficult. However, the calculations have not

been taken further at this time due to the variability of the behavior observed.

The brittleness of the TiAl in tension contrasted with relative ductility in compression may be discussed in view of the active deformation modes that were detected in this investigation. It has been suggested by Cass and Spencer[3] that the brittleness is due to the limited number of glide systems available as these workers did not detect any a/2[011] dislocations or the a/6⟨112⟩ stacking faults. Fig. 16 presents a representative quadrant of the stereographic projection for the Llo structure. Superimposed on this figure are the directions along which tensile or compressive load should be applied to a single crystal in order to achieve Schmid factors equal to 0.5 and 0.4 for the slip systems of the type (111)(11$\bar{0}$). Load applied along the [100] direction will activate 4 slip systems of this type with Schmid factors equal to about 0.4; by moving the load axis towards [101] two systems will be favored, while the other two will have Schmid factor equal to only about 0.3 or less. Load applied in other directions will probably not activate any "easy" slip system. Four slip systems (of which only three are independent) that are activated only by loading in a specific direction may not be sufficient for the plastic deformation of a random polycrystal.

Twinning plays an important role in the plastic deformation of TiAl. Only four types of twins are available and the equi-Schmid factor lines for them are shown in Fig. 17. The lines on the stereographic projection are of two kinds—single lines for compression and double lines for tensile load. Compressive load along the [001] direction will activate all four twinning systems, however, a tensile load in the general direction of [110] or [11$\bar{0}$] will activate only two twin systems at a time. This last fact may contribute to the difference in ductility in tension and in compression.

Equi-Schmid factor lines for the (111)[10$\bar{1}$] type dislocations are shown in Fig. 18. It had been assumed that the APB associated with such dislocations would make the nucleation and movement of such defects more difficult and thus this would be a "hard" deformation mode. As no direct information on the relative critical resolved shear stresses has been obtained at this time, (See Ref. 3 for the experimental difficulties associated with the growth of single crystals of the γ-phase) no further conclusion can now be drawn. It can be seen from Fig. 18 that the (111)[10$\bar{1}$] type glide essentially fill in the stereographic triangle and if such dislocations are mobile at stresses comparable to the other system, the material should be ductile. The fact remains, however, that TiAl cleaves at stresses below the macroscopic flow stress (determined in compression) and, thus, we are left with the observation that although sufficient slip systems are present and the material is soft (in a hardness test), the anisotropy of glide cannot be used to explain the brittleness problem. The influence of test temperature, prestrain, and so forth, is under study at this time to delineate the extent of this brittleness and potential methods of overcoming it.

CONCLUSIONS

The study of the deformation modes in the TiAl phase active during compression testing at ambient temperatures has revealed that:

1) The "hard" slip mode a/2[011] type dislocations have been detected. The structure and contrast behavior of such dislocations are not consistent with that predicted for Llo lattices.

2) A large number of a/2[110] type dislocations are formed, the structure and contrast behavior of these dislocations are as predicted.

3) a/2[011] dislocations generate a/6[112] type partials producing numerous stacking faults which are related to the profuse [112][111] twinning that also is observed.

4) Anisotropy of glide cannot be used to explain the brittleness of TiAl at this time. Further work on the CRSS required to activate the various glide systems, coupled with an analysis of cleavage crack nucleation and growth may clarify this point.

ACKNOWLEDGMENTS

The authors are grateful to Mr. A. M. Adair and F. J. Gurney of the Air Force Materials Laboratory for extruding the alloys; to Mr. M. M. Allen of Pratt and Whitney, Florida for supplying materials; and to Mr. T. F. Orcutt, Mr. J. V. Smith, and Mr. D. F. Frank for technical assistance. We also wish to thank Dr. L. A. Jacobson for his critical reading of this paper.

One of us, D. Shechtman, is grateful to the N.R.C. for a resident research associateship.

REFERENCES

1. J. B. McAndrew and H. D. Kessler: *J. Metals*, 1956, vol. 8, p. 1348.
2. M. J. Marcinkowski, N. Brown, and R. M. Fisher: *Acta Met.*, 1961, vol. 9, p. 129.
3. T. R. Cass and W. R. Spencer: Technical Report AFML-TR-69-293, Dec. 1969.
4. D. W. Pashley, J. L. Robertson, and M. J. Stowell: *Phil. Mag.*, 1969, vol. 19, p. 83.
5. M. J. Blackburn and J. C. Williams: *Trans. TMS-AIME*, 1967, vol. 239, p. 287.
6. M. J. Blackburn: *The Science Technology and Application of Titanium*, R. Jaffee and N. Promisel, eds., Pergamon Press, 1970.
7. E. Ence and H. Margolin: *Trans. TMS-AIME*, 1961, vol. 221, p. 151.
8. M. J. Marcinkowski: *Electron Microscopy and Strength of Crystals*, G. Thomas and J. Washburn, eds., Interscience Publishers, 1963.